

## RESEARCH ARTICLE

10.1002/2017JD026699

## Key Points:

- First high-resolution centennial-scale (1810–2004 A.D.) dust record from Miaoergou Glacier, eastern Tien Shan
- Regional factors affecting dust flux include precipitation, spring soil moisture, and spring surface wind speed
- The NAO is a potential key driver of dust emissions over the arid regions in the northwestern China

## Supporting Information:

- Supporting Information S1
- Data Set S1

## Correspondence to:

S. Hou,  
shugui@nju.edu.cn

## Citation:

Zhang, W., S. Hou, Y. Liu, S. Wu, W. An, H. Pang, and C. Wang (2017), A high-resolution atmospheric dust record for 1810–2004 A.D. derived from an ice core in eastern Tien Shan, central Asia, *J. Geophys. Res. Atmos.*, 122, 7505–7518, doi:10.1002/2017JD026699.



Received 22 FEB 2017

Accepted 6 JUL 2017

Accepted article online 8 JUL 2017

Published online 24 JUL 2017

# A high-resolution atmospheric dust record for 1810–2004 A.D. derived from an ice core in eastern Tien Shan, central Asia

Wangbin Zhang<sup>1</sup>, Shugui Hou<sup>1,2</sup> , Yaping Liu<sup>3</sup>, Shuangye Wu<sup>1,4</sup> , Wenling An<sup>5</sup>, Hongxi Pang<sup>1</sup>, and Chaomin Wang<sup>1</sup>

<sup>1</sup>School of Geographic and Oceanographic Sciences, Nanjing University, Nanjing, China, <sup>2</sup>CAS Center for Excellence in Tibetan Plateau Earth Sciences, Beijing, China, <sup>3</sup>State Key Laboratory of Cryospheric Sciences, Northwest Institute of Eco-Environment and Resources, Chinese Academy of Science, Lanzhou, China, <sup>4</sup>Department of Geology, University of Dayton, Dayton, Ohio, USA, <sup>5</sup>Institute of Geology and Geophysics, Chinese Academy of Science, Beijing, China

**Abstract** Centennial-scale, high-resolution records of atmospheric dust conditions are rare in the arid and semiarid regions of central Asia, limiting our understanding of the regional climate and environmental changes and their potential driving forces. In this paper, we present an annually resolved atmospheric dust record covering the period of 1810–2004 A.D., reconstructed from an ice core retrieved at 4512 m above sea level from the Miaoergou Glacier in the eastern Tien Shan. The time series of dust flux for the past 195 years shows three periods of relatively low values (i.e., 1810–1829 A.D., 1863–1940 A.D., and 1979–2004 A.D.) and two periods of relatively high values (i.e., 1830–1862 A.D. and 1941–1978 A.D.). Spatial correlation analysis suggests possible regional factors controlling the dust flux, including antecedent summer precipitation, spring soil moisture, and near-surface wind speed. In addition, the Miaoergou dust flux is closely associated with the winter index of the North Atlantic Oscillation (NAO) over the past two centuries, with high (low) dust periods coinciding with the negative (positive) phases of the NAO. The persistent relationship suggests that the NAO may have been a key driver on dust flux change over the arid regions between the Tien Shan and Kunlun Mountains.

## 1. Introduction

Aeolian dust, mostly emitted from bare soils in the arid and semiarid regions, is a key atmospheric constituent and represents an important natural source of atmospheric particulate matter. It is the most important aerosol by mass in comparison to black carbon, organic carbon, and brown carbon from combustion of fossil fuels, sea spray from sea surface, and ash from volcanic eruptions [Ginoux *et al.*, 2012; Intergovernmental Panel on Climate Change, 2013]. Dust plays an important role in the Earth's radiation balance, biogeochemical and hydrological cycles, and human society [Jickells *et al.*, 2005]. Dust absorbs and scatters incoming shortwave (solar) radiation and can thus affect air temperature [Claquin *et al.*, 1999; Ji *et al.*, 2016]. Wind-transported dust is a major source of iron and other limiting nutrients that control ocean productivity [Jickells *et al.*, 2005]. It can affect cloud properties and precipitation patterns [Rosenfeld *et al.*, 2001]. Small dust particles are harmful to human respiratory health [Griffin *et al.*, 2001]. Therefore, it is important to understand spatial and temporal variation of dust concentration and its underlying driving forces.

Asian dust mainly originates in the arid and semiarid regions in central Asia (the northwestern China and deserts of Mongolia), with the largest dust production during spring [Prospero *et al.*, 2002]. Mineral dust is then transported over the Eurasian continent by northwesterly winds near the surface and by westerly winds over the Pacific Ocean in the free troposphere [Parungo *et al.*, 1994; Sun *et al.*, 2001; Uno *et al.*, 2009]. Traditionally, variability of dust aerosol over central Asia and its relationship with climate change have been studied via ground-based and satellite measurements. However, as in situ and satellite observations are commonly scarce and limited either in time or space, most existing studies have been performed over short temporal periods and/or small regional scales [Ding and Li, 2005; Gao and Washington, 2010; Zhao *et al.*, 2013].

Ice core records offer the potential to reconstruct high-resolution long-term records of past atmospheric dust concentrations [Kang *et al.*, 2003, 2010; Thompson *et al.*, 2000; Zhang *et al.*, 2015]. The vast extent of glaciers in the mountains of central Asia provides a means to measure the depositional flux of atmospheric dust over a wide geographic area [Xu *et al.*, 2007]. Previous studies indicate considerable differences in climatic and environmental change at various regions of central Asia. For example, the dust content in the Dasuopu ice

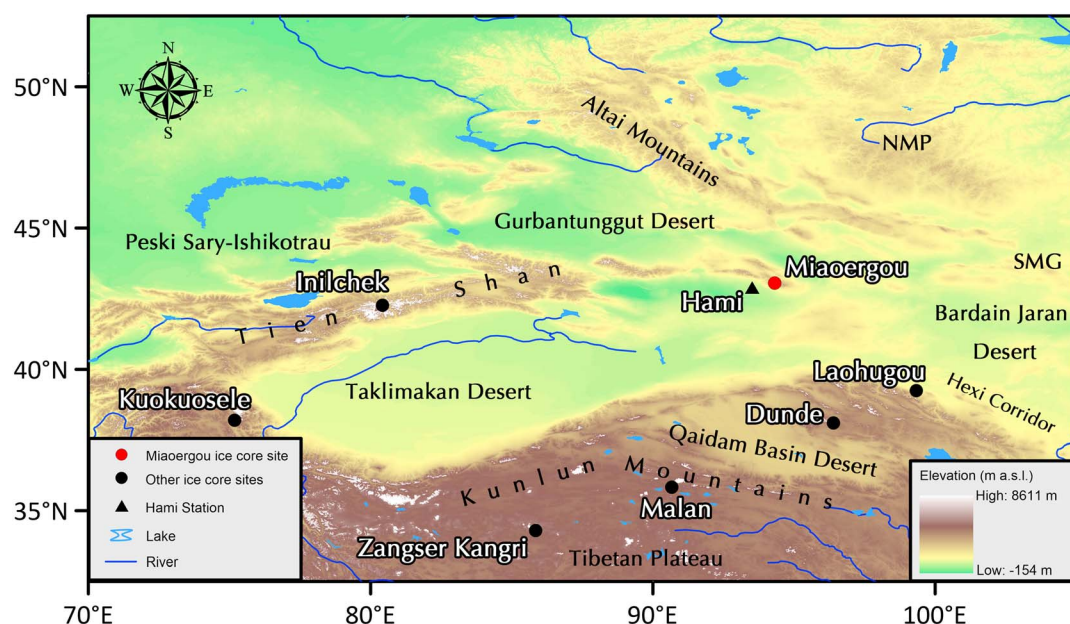


**Figure 1.** Map of the Miaoergou ice core drilling site and other ice core sites mentioned in the text. The topographic data were extracted using ETOPO1 elevations global data (<https://www.ngdc.noaa.gov/mgg/global/global.html>). SMG: Southern Mongolian Gobi, NMP: Northern Mongolian Plateau.

core [Thompson *et al.*, 2000] in the southern Tibetan Plateau (TP) has increased over the past 1000 years, suggesting a strengthening of dust storm activities. The Tanggula ice core in the central TP showed high dust fluxes during 1860 A.D. to 1874 A.D. [Wu *et al.*, 2013]. The Geladaidong ice core in the central TP showed high dust concentrations in the eighteenth and nineteenth centuries and low concentrations in the twentieth century [Grigholm *et al.*, 2015; Zhang *et al.*, 2015]. The Inilchek ice core in central Tien Shan showed the highest dust concentrations during the 1950s to 1970s and lower dust concentration since the 1980s [Grigholm *et al.*, 2017].

Tien Shan is located in a remote area of central Asia, surrounded by important dust source areas (Figure 1): the Taklimakan desert (the world's second largest shifting sand desert) in the south, the Southern Mongolian Gobi and the Northern Mongolian Plateau in the east, the Gurbantunggut desert in the northwest, and the Peski Sary-Ishikotrau desert in the west [Liu *et al.*, 2011]. Therefore, the ice core records from this region can offer an opportunity to understand the environmental changes over the most important dust sources in central Asia. In Tien Shan, previous studies on aeolian dust have been limited, with the longest available records representing only 88 years (1908–1995 A.D.) [Grigholm *et al.*, 2017]. In this study, we present a 195 year atmospheric dust deposition record (1810–2004 A.D.) developed from a shallow ice core retrieved from the Miaoergou Glacier located in eastern Tien Shan (Figure 1). We first trace the potential sources of dust deposited at the Miaoergou Glacier. We then investigate the relationship between the Miaoergou dust record and regional climatic factors, including precipitation, soil moisture, and surface wind speed. Finally, we examine the impact of the antecedent winter North Atlantic Oscillation (NAO) on the Miaoergou dust record during the past two centuries.

## 2. Study Site

The Miaoergou Glacier is one of the many glaciers in eastern Tien Shan and is located in the northern part of the Hami Basin south of the Karlik Mountain, covering an area of 3.45 km<sup>2</sup>. It is the eastmost glacier in Tien Shan. The glacier's altitude ranges from 4512 m above sea level (asl) at its summit to 3840 m asl at the ice tongue, and the equilibrium line lies at ~4100 m asl [Shi *et al.*, 2008]. Climatic conditions are dominated by the strengths and interactions of westerly cyclones and Siberian High [Aizen *et al.*, 1997]. During the warm summer season, the westerlies transport large amount of water vapor from the Aral-Caspian closed basin, the eastern Mediterranean Sea, the Black Sea, and the North Atlantic to this glacier [Aizen *et al.*, 2006].

During the cold winter season, precipitation of eastern Tien Shan is minimal due to dominant influence of the Siberian High circulation system [Liu *et al.*, 2011].

### 3. Materials and Methods

#### 3.1. Retrieval and Analysis of the Miaoergou Ice Core

In August 2005, two ice cores to bedrock (58.7 m for Core 1 and 57.6 m for Core 2, respectively) were retrieved from a dome on the Miaoergou Glacier (43°03′19″N, 94°19′21″E, 4512 m asl). The low borehole temperature at the drilling site (−7.2°C at 10 m depth and −8.2°C at the bottom) is beneficial for the preservation of the ice core records [Liu *et al.*, 2009]. The ice cores were transported frozen to the State Key Laboratory of Cryospheric Sciences (SKLCS, Chinese Academy of Sciences, Lanzhou, China) for processing and analyses. This study is based on the records obtained from Core 2. Core 2 (~9.4 cm in diameter) was split axially into two equal halves. One half was stored for archival purposes; the other was sampled continuously at an interval of ~5 cm in a cold room (−20°C). A total of 1205 sections was obtained for the measurements of trace elements, stable isotopes, major ions, and insoluble particles. The samples for stable isotopes were cut axially from both sides (~1 cm for each side) at each section. The inner sections were placed into clean low-density polyethylene (LDPE) bags for further decontamination. The decontamination procedures were performed in a class 100 laminar flow clean bench, located inside a cold room at −12°C. Operators wore nonparticulating clean suits and LDPE gloves. The gloves were replaced frequently as needed. Each core section was handled in a series of steps. First, ~5 mm of ice was shaved off from each end with a clean stainless steel scalpel. The core section was then placed in the lathe, and the first ~5 mm thick veneer layer was shaved off with a clean stainless steel scalpel. Next, the operator changed LDPE gloves and shaved off a second veneer layer with a new clean stainless steel scalpel. This procedure was repeated, and the third veneer layer was shaved off with a clean ceramic knife. The remaining part of the core section was then held with polypropylene tongs, and an additional ~5 mm of ice was shaved off from each end of the core with a clean ceramic knife. Finally, the remaining inner core section was placed in a clean LDPE bag for trace element, insoluble particle, and major ion measurement. The ice chips shaved off during decontamination were collected at an interval of ~2.80 m from the entire core for  $^{210}\text{Pb}$  measurement (with a total of 18 samples). They were also collected at an interval of 0.50 m for the upper 41.20 m of the core for  $\beta$  activity measurement (with a total of 81 samples).

The  $\delta^{18}\text{O}$  content of the ice core was measured on an Isotopic Ratio Mass Spectrometer (ThermoFinnigan MAT 252, Bremen, Germany) in the SKLCS, using the classical  $\text{CO}_2$  equilibration technique. The results are expressed in  $\delta^{18}\text{O}$  on the Vienna Standard Mean Ocean Water 2 scale with an overall uncertainty of  $\pm 0.05\text{‰}$  [Liu *et al.*, 2011]. The  $\beta$  activity measurements were performed using a MINI 20 Alpha-Beta Multidetector (Eurisys Mesures, St. Quentin, France) in the SKLCS. Major cations and anions were analyzed using a Dionex 600 and ICS-2500 ion chromatograph (with a detection limit of  $1 \text{ ng g}^{-1}$ ), respectively. The trace elements (V, Cr, Mn, Co, Ni, Cu, As, Rb, Sr, Mo, Cd, Sn, Sb, Ba, Tl, Pb, Bi, Th, and U) were measured at the Korea Polar Research Institute, Korea, on an Inductively Coupled Plasma Mass Spectrometer (Perkin Elmer Sciex, ELAN 6100). Detailed information on the instrument setting and optimization was described by Lee *et al.* [2008]. The  $^{210}\text{Pb}$  activity was indirectly analyzed by measuring the  $\alpha$  decay of  $^{210}\text{Po}$  at an energy of 5.3 MeV using alpha spectrometry (ORTEC, Oak Ridge, Tennessee) at the University of Bern, Switzerland. Detailed analytical procedures and accuracy were described in Wang *et al.* [2014].

Dust concentration and size distribution were measured using a particle counter (Coulter Counter© Multisizer III, Beckman Coulter Inc., Fullerton, CA, USA) setup in a class 100 clean hood in a class 1000 clean room in the SKLCS. The instrument works on the basis of detecting the electric signal generated by particles forced to flow through a small aperture tube (50  $\mu\text{m}$  in diameter). Samples were melted immediately prior to the particle analysis. Samples of 2.50 mL were extracted from the containers using a pipette and diluted 1:4 with NaCl electrolyte for particle counting. The instrument was set to detect particles with an equivalent spherical diameter larger than 1.0  $\mu\text{m}$ . Three consecutive measurements were performed on each sample to ensure the accuracy of the results. Results were then averaged for individual samples, yielding an estimated error of <10% on particle number concentrations. Routine analysis of filtered deionized water blanks showed background counts to be on average 10 times lower than the lowest number concentration in the samples. Particle mass concentration was calculated from the volume sums, assuming a mean particle density of  $2.50 \text{ g cm}^{-3}$  [Xu *et al.*, 2007].

The Miaoergou depth-age scale is presented in Figure S1 in the supporting information. The ice core was annually dated back to 1810 A.D. using seasonal variations of the Miaoergou ice core chemical records, including  $\delta^{18}\text{O}$ ,  $\text{Ca}^{2+}$ , and Ba [Liu *et al.*, 2011; Wang *et al.*, 2016]. Furthermore, the timescale was verified using  $\beta$  activity and  $^{210}\text{Pb}$ . Wang *et al.* [2016] provide detailed information on the depth-age scale including dating uncertainties of  $\pm 1$  year at 1963 A.D. (16.80 m) and  $\pm 8$  years at 1810 A.D. (40.11 m).

### 3.2. Meteorological and Climate Data

Station-based monthly mean dust occurrence frequency (dust storm d month<sup>-1</sup>) data were extracted from the China Strong Dust Storm Data Set (1960–2004 A.D.) (<http://data.cma.cn/en>) and used for comparison with the Miaoergou ice core dust records. We selected 48 meteorological stations located on the northwestern China. Dust occurrence used in this paper includes three phenomena: dust haze, blowing dust, and dust storms (according to the definition by the National Climate Center, China Meteorological Administration). The data have been processed to ensure good consistent quality and are widely used [Fan and Wang, 2004; Zhu *et al.*, 2008].

Climate data on precipitation, soil moisture, self-calibrating Palmer Drought Severity Index (scPDSI), and surface wind speed were collected in order to investigate the influence of regional climatic factors on the Miaoergou ice core records. The monthly precipitation data with a  $0.5^\circ \times 0.5^\circ$  resolution (1901–2004 A.D.) were obtained from the Climate Research Unit at the University of East Anglia (CRU TS v. 3.24) [Harris *et al.*, 2014]. The monthly mean soil moisture data were obtained from the monthly Global Land Data Assimilation System version 2 product (GLDAS-2), with a  $1.0^\circ \times 1.0^\circ$  resolution [Rodell *et al.*, 2004]. The data contain soil moisture at four vertical layers from the surface to 200 cm below. The depths of the four soil layers are from 0 to 10 cm, 10 to 40 cm, 40 to 100 cm, and 100 to 200 cm. Soil moisture is expressed in volume ( $\text{m}^3/\text{m}^3$ ). GLDAS-2 is a global, high-resolution, offline land data assimilation system developed jointly by the National Aeronautics and Space Administration/Goddard Space Flight Center and the National Oceanic and Atmospheric Administration/National Centers for Environmental Prediction (NOAA/NCEP). The GLDAS-2 data set were widely used in data assimilation, validation, weather and climate model initialization, and hydrology [Bi *et al.*, 2015; Kim and Choi, 2015]. The scPDSI data with a  $0.5^\circ \times 0.5^\circ$  resolution (1901–2004 A.D.) are available at <https://crudata.uea.ac.uk/cru/data/hrq/>. The scPDSI is calculated from time series of precipitation and temperature, together with fixed parameters related to the soil/surface characteristics at each location [Osborn *et al.*, 2016; Schrier *et al.*, 2013]. The station-based monthly wind speed data were obtained from the China Meteorological Data Service Center (1960–2004 A.D.) (<http://data.cma.cn/en>).

To analyze the influence of atmospheric circulation systems on the Miaoergou ice core records, the National Centers for Environmental Prediction/National Center for Atmospheric research (NCEP/NCAR) reanalysis data with a  $2.5^\circ \times 2.5^\circ$  resolution (1948–2004 A.D.) were used [Kalnay *et al.*, 1996]. The NCEP/NCAR reanalysis data are available at <http://www.esrl.noaa.gov/psd/data/gridded/>.

Finally, the Miaoergou ice core records were compared with the observed and reconstructed North Atlantic Oscillation (NAO) indices to explore their potential connections [Ortega *et al.*, 2015; Luterbacher *et al.*, 2001; Vinther *et al.*, 2003]. The observed NAO and reconstructed NAO indices were obtained from the World Data Center Paleo archive at the NOAA (<https://www.ncdc.noaa.gov/paleo/>).

## 4. Results and Discussion

### 4.1. Dust Flux and Size Distribution

Figures 2a and 2b show the annual dust concentration and depositional flux, respectively, in the Miaoergou ice core. Dust depositional flux is calculated as dust concentration multiplied by the ice/snow accumulation rate. Dust concentration and flux data are highly consistent with each other ( $n = 195$ ,  $r = 0.78$ ,  $p < 0.001$ ). Therefore, in the remaining of the paper, we focus the discussion on the annual dust flux to facilitate direct comparison with other studies. The annual dust flux of the Miaoergou ice core ranges from 9.12 to 1581.91  $\mu\text{g cm}^{-2} \text{a}^{-1}$  with a mean value of 267.20  $\mu\text{g cm}^{-2} \text{a}^{-1}$  and a median value of 199.24  $\mu\text{g cm}^{-2} \text{a}^{-1}$ . Robust splines were calculated (tension 0.01) to remove short-term interannual variability and assess decadal-scale trends [Grigholm *et al.*, 2015]. The time series reveals large increase of atmospheric dust concentration since the 1830s, followed by large decline during the period 1850–1860 A.D. Dust flux maintains



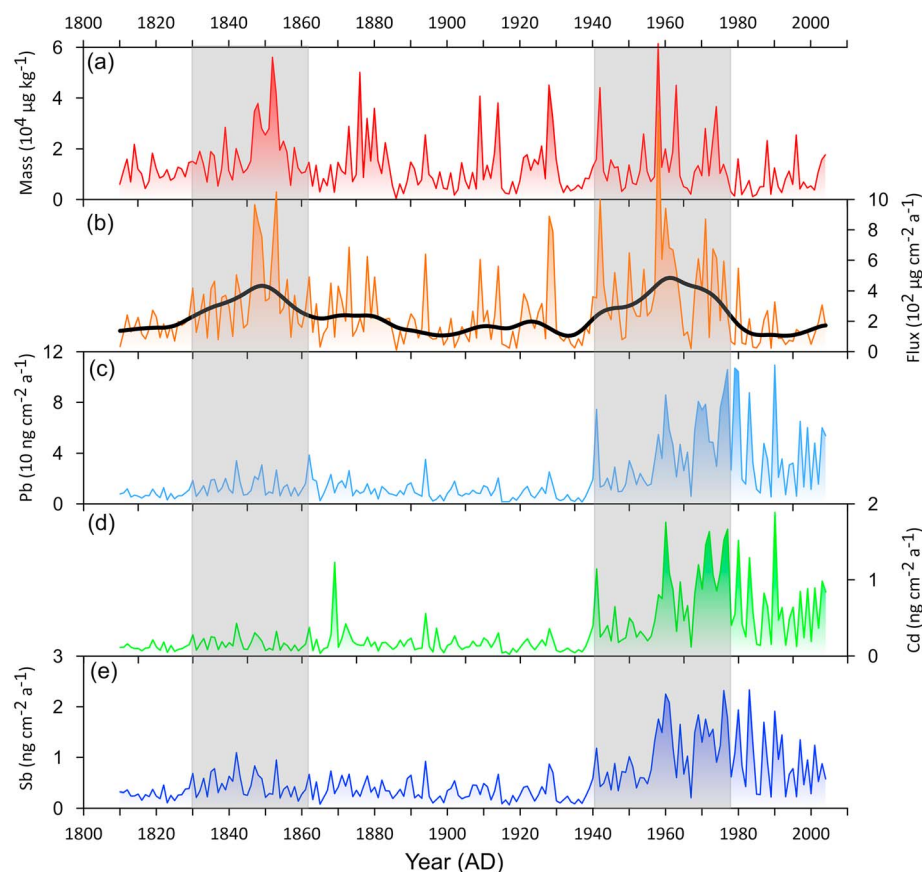


**Figure 2.** (a) Annual mean mass concentration, (b) annual mean fluxes of dust, (c) Pb, (d) Cd, and (e) Sb. Black line in Figure 2b represents robust splines smoothing (tension 0.01).

relatively low since the 1860s but starts to increase since the 1940s, followed by a decline since the 1960s and through the end of the record.

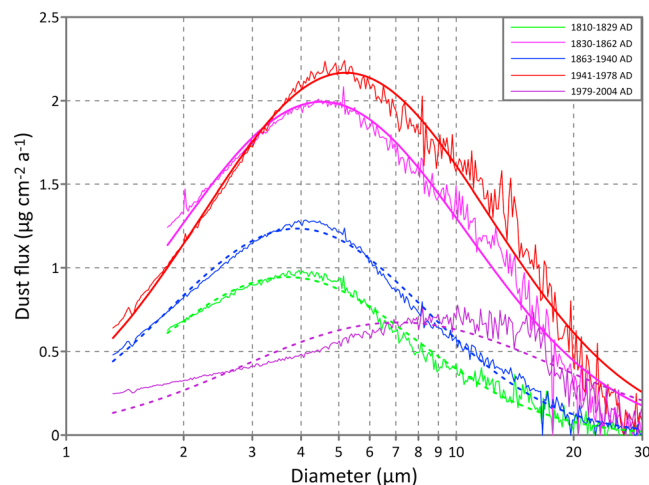


**Figure 3.** The dust particle size distributions for five dust stages. Thin lines represent the original data, and thick lines indicate the fitted lognormal distribution functions. Solid lines indicate periods with high dust fluxes, and dashed lines indicate those with low dust fluxes.

Based on the smoothed data, five dust stages can be identified over the past 195 years: three low dust periods: 1810–1829 A.D. ( $158.32 \mu\text{g cm}^{-2} \text{a}^{-1}$  on average), 1863–1940 A.D. ( $207.91 \mu\text{g cm}^{-2} \text{a}^{-1}$  on average), and 1979–2004 A.D. ( $137.55 \mu\text{g cm}^{-2} \text{a}^{-1}$  on average) and two high periods: 1830–1862 A.D. ( $381.40 \mu\text{g cm}^{-2} \text{a}^{-1}$  on average) and 1941–1978 A.D. ( $433.36 \mu\text{g cm}^{-2} \text{a}^{-1}$  on average) (Figure 2b). The average dust-size distribution of these five stages was presented in Figure 3. Almost all the dust particle size distributions during the period 1810–1978 A.D. fit a lognormal distribution (Figures 3 and S2). The mode values between 1810 A.D.

and 1978 A.D. range from 2.6 to 9.6  $\mu\text{m}$ , with a mean value of 4.7  $\mu\text{m}$  and a median value of 4.1  $\mu\text{m}$ , which are typical of mineral particles deposited in alpine snowfields with a transport distance of several hundred kilometers [Wake and Mayewski, 1994; Wu *et al.*, 2010b; Xu *et al.*, 2016] but much coarser than those of Himalayan ice cores [Wake and Mayewski, 1994; Xu *et al.*, 2010]. Particles with  $d > 15 \mu\text{m}$ , considered as originating from local sources, contribute to 5.1% of dust flux at Miaoergou, similar to that found at the Dundee (8.2%) [Wu *et al.*, 2010b], suggesting that the local material contributes little to the dust mass at the Miaoergou Glacier. In addition, it is clear that within the two respective high (1830 A.D. to 1862 A.D. and 1941 A.D. to 1978 A.D.) and low dust (1810 A.D. to 1829 A.D. and 1863 A.D. to 1940 A.D.) periods, the particle size distributions are fairly consistent. This suggests that climate and environment conditions during the two respective high and low dust stages are very similar. In contrast, the dust particle size distribution during the period 1980–2004 A.D. does not fit a lognormal distribution well, mostly exhibiting a low positive slope with particles existing sparsely in higher channels (Figure 3). The mode value during the fifth stage (1979 A.D. to 2004 A.D.) is 7.9  $\mu\text{m}$  (Figure 3). The contribution of dust particles with  $d > 15 \mu\text{m}$  to dust flux is high (15.6%), compared with the other two low dust stages (3.6% for 1810–1829 A.D. and 4.3% for 1863–1940 A.D.). The abnormal distributions during the fifth stage may be associated with increased dust emissions from local sources. For example, between 1985 A.D. and 1995 A.D., the energy production and consumption (primary coal) increased by  $\sim 30\%$  and  $\sim 50\%$ , respectively, in Xinjiang Province [Grigholm *et al.*, 2016]. This increase could contribute to the higher concentration of coarse particles to dust flux at Miaoergou. Another possible explanation is the dramatic increase of heavy metal concentration in the atmosphere over the past several decades in central Asia [Grigholm *et al.*, 2016]. Heavy metals can be absorbed by fly ash particles and lead to the increase of the particle size of fly ash [Meji, 1994] and contribute to higher concentration of coarse particles to dust flux at Miaoergou. This explanation is also supported by our ice core data, which show increased fluxes of heavy metals (e.g., Pb, Sb, and Cd) in the past several decades (Figure 2).

The Miaoergou dust records are compared with dust data derived from other ice cores in the arid areas over central Asia, including Inilchek [Grigholm *et al.*, 2016], Laohugou [Dong *et al.*, 2013], Dundee [Thompson *et al.*, 2006], Malan [Wang, 2005], Kuokuosele [Tenzin *et al.*, 2016], and Zangser Kangri [Zhang *et al.*, 2016] (Figure S3). Most of these records show a decreasing trend for dust records for various time periods. Both Miaoergou and Laohugou show significant declining trends since the 1960s: Miaoergou (1960–2004 A.D.,  $r^2 = 0.31$ ,  $p < 0.005$ ) and Laohugou (1960–2004 A.D.,  $r^2 = 0.36$ ,  $p < 0.005$ ). Inilchek shows a continuous decline in dust since the 1950s (1950–1995 A.D.,  $r^2 = 0.20$ ,  $p < 0.01$ ). Malan shows a decreasing trend since the 1850s (1850–2000 A.D.,  $r^2 = 0.46$ ,  $p < 0.005$ ). Kuokuosele shows a decreasing trend since 1908 A.D. (1908–2010 A.D.,  $r^2 = 0.34$ ,  $p < 0.005$ ). Dundee shows a long-term decline in dust since the 1850s until the 1980s (1850–1980 A.D.,  $r^2 = 0.30$ ,  $p < 0.005$ ), when it starts to increase. Zangser Kangri shows a decline during 1980–2004 A.D. ( $r^2 = 0.16$ ,  $p < 0.05$ ) and starts to increase since the late 1980s. It was clear that the Miaoergou dust records were more similar to those from the northeastern TP (i.e., Laohugou). The variability of dust records in these ice cores could be caused by differences in dust source regions, moisture trajectories, atmospheric circulation, and mountain meteorology that govern these ice cores [Kang *et al.*, 2010; Xu *et al.*, 2010].

#### 4.2. Possible Dust Source and Transport Route

Based on the Sr-Nd isotopic compositions of insoluble particles, Du *et al.* [2015] suggested that the Taklimakan desert and Gobi desert are the primary dust sources for the Miaoergou Glacier. The Sr-Nd isotopic compositions of dust from the Miaoergou ice core and those from other central Asia regions are reported in Figure S4 and Text S1. [Chen *et al.*, 2007; Rao *et al.*, 2015; Wu *et al.*, 2010a; Xu *et al.*, 2009, 2012; Zhao *et al.*, 2015]. In addition, back trajectory analysis of air masses also indicates that most trajectories at the Miaoergou site originate from the west (Figure 4), supporting the Taklimakan provenance of the Miaoergou dust.

To further confirm this, we performed the spatial correlations between the Miaoergou dust flux and the annual dust day records from the meteorological stations over the northwestern China for the period 1960–2004 A.D. (Figure S5). The areas with significant positive correlations are located in the western Taklimakan desert, the Gobi desert, and the Hexi Corridor. The western Taklimakan desert is most important because of its frequent dust storms [Sun *et al.*, 2001]. The correlation coefficient with the Miaoergou dust flux

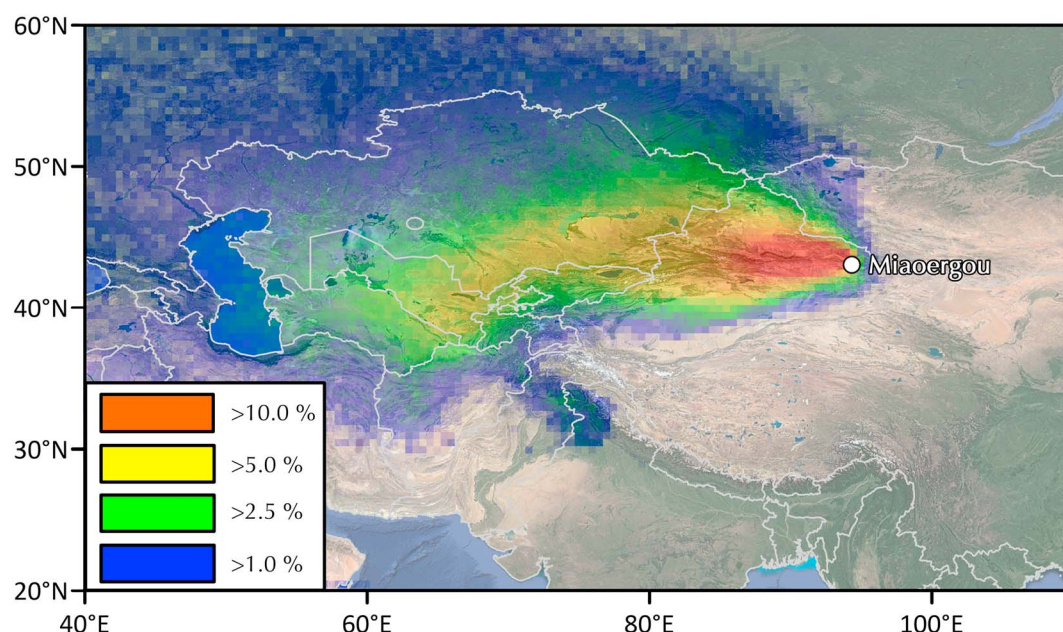


**Figure 4.** Frequency plot of 7 day back trajectories during the season of high dust storm activity (March–May) between 1948 A.D. and 2004 A.D. Back trajectories were run every 6 h (with a total of 20,976 trajectories). The white dot indicates the Miaoergou ice core site. The back trajectory data are from the U.S. National Oceanic and Atmospheric Administration (NOAA) (available at <http://arlftp.arl.hq.noaa.gov/pub/archives/reanalysis>).

is 0.46 ( $p < 0.01$ ) for the Hami meteorological station close to our coring site in eastern Tien Shan and 0.48 ( $p < 0.01$ ) for the averaged dust day records of the 16 meteorological stations around the Taklimakan desert. We therefore think that the Miaoergou ice core record could serve as a proxy for dust emissions over the deserts between Tien Shan and Kunlun Mountains.

### 4.3. Climate Factors

To help understand the physical mechanisms responsible for the variability in atmospheric dust at Miaoergou, the annual Miaoergou dust flux was correlated to climate variables during high-frequency dust storm season (March–May). To minimize the influence of coarse particles, dust particles with  $d > 15 \mu\text{m}$  were removed from the correlation analyses. In addition, we use the log transformation instead of the original dust flux values in the correlation analysis, because the independent factors affect the Miaoergou dust fluxes in multiplicative way.

#### 4.3.1. Drought Conditions Over the Dust Source Regions

High interannual variability in precipitation is a typical characteristic of central Asia climates, and it tends to produce extreme conditions, such as severe droughts, which significantly affect the dust emission [Liu *et al.*, 2004]. Results of correlation analysis of the seasonal and annual precipitation with the Miaoergou log-Dust time series suggest that the Miaoergou log-Dust is negatively correlated to precipitation of the antecedent seasons in the arid regions of the northwestern China, especially to the precipitation of the antecedent summer (Figure 5a). The areas with the strongest negative correlations are located in the Gobi desert and the eastern Taklimakan desert, two main source regions of dust deposited in the Miaoergou Glacier. This suggests that the high dust emissions over the northwestern China are closely associated with the negative precipitation anomalies over this region, and vice versa. Although correlations of the Miaoergou log-Dust with the antecedent fall (Figure S6a), winter (Figure S6b), and concurrent spring (Figure S6c) are relatively weak, the spatial correlation pattern of annual precipitation (Figure 5b) is similar to that of the preceding summer precipitation. In addition, the correlation is slightly stronger between the Miaoergou log-Dust and annual precipitation (from the previous summer to spring of the current year) than antecedent summer precipitation in the Gobi desert and the eastern Taklimakan desert. This indicates that the summer precipitation anomaly dominates the overall variability of precipitation of the whole year, but the cumulative effect of the precipitation anomaly of the entire year may be a more important factor to the dust emission.



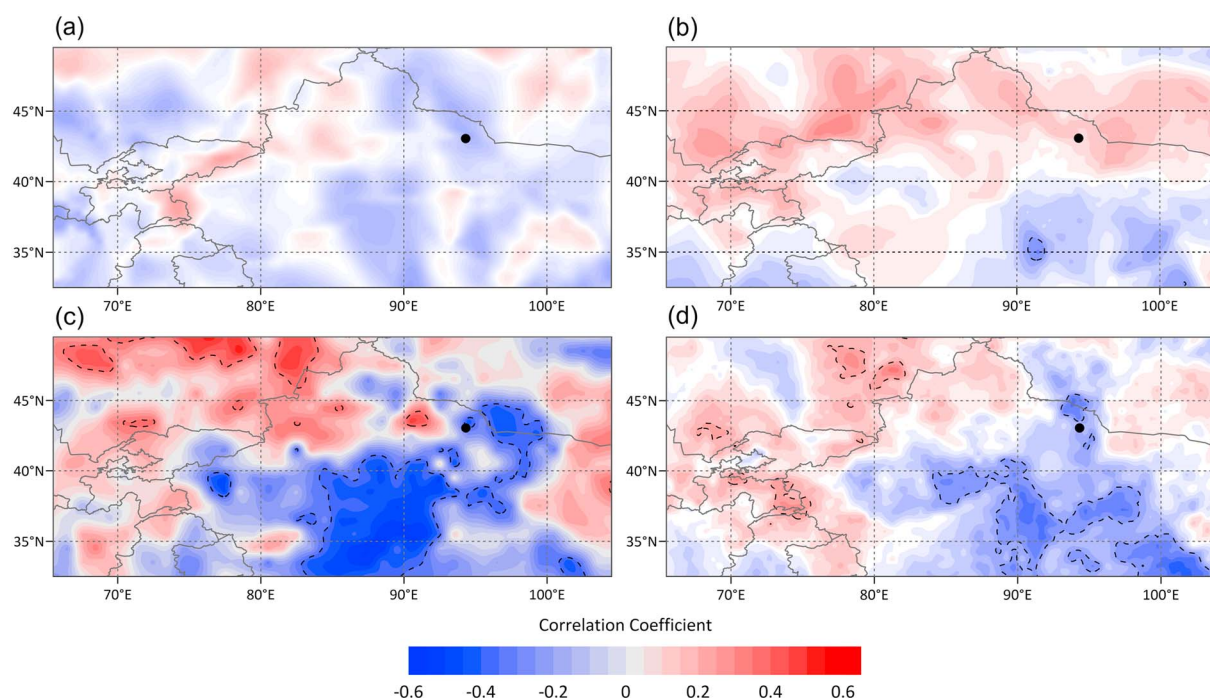


**Figure 5.** (a) Spatial correlations between the Miaoergou log-Dust and antecedent summer precipitation (1901–2003 A.D.), (b) antecedent annual precipitation (1901–2004 A.D.), (c) spring soil moisture (1948–2004 A.D.), and (d) reconstructed scPDSI (1901–2004 A.D.). The regions circled by black dashed lines represent grids where correlation is significant at the 99% confidence level. The black dot indicates the Miaoergou ice core site.

Another crucial factor controlling the dust events is soil moisture conditions in the dust source region [McTainsh *et al.*, 1998]. In arid and semiarid regions, the vigor of vegetation is very sensitive to soil moisture conditions [Liu *et al.*, 2004]. Moreover, except in conditions of extreme cold or in the presence of coarse soil particles, soil moisture conditions determine the threshold friction velocity for a dust outbreak on bare soil, because soil moisture increases the cohesive forces between soil particles; therefore, moistened sand requires higher wind speed to generate a dust event [Kim and Choi, 2015]. We examined the relationships of the Miaoergou log-Dust to soil moisture conditions during the high-frequency dust storm season (March–May) over the 1948–2004 A.D. The spatial patterns of correlation coefficients between the Miaoergou log-Dust and the soil moisture conditions (Figure 5c) are similar to those of the precipitation data (Figures 5a and 5b). There are two centers of high correlations: the western portion of the China–Mongolia border and the eastern Taklimakan desert. Remarkably, compared with the antecedent summer precipitation, the spring soil moisture conditions show a higher correlation with the Miaoergou log-Dust. This is plausible as soil moisture anomalies have a strong persistence from the antecedent summer to the following spring, with a more direct influence on emission of dust in spring [Liu *et al.*, 2004]. To investigate whether the drought conditions may have a long-term influence on the dust emission, we calculated the correlations of the Miaoergou log-Dust and the constructed drought index (scPDSI) during the 1901–2004 A.D. [Osborn *et al.*, 2016; Schrier *et al.*, 2013]. The spatial pattern of the correlation between the Miaoergou log-Dust and the scPDSI (Figure 5d) is quite similar to that of the soil moisture (Figure 5c). This indicates that the drought conditions may have a persistent influence on the dust emission over the source regions of the Miaoergou dust.

#### 4.3.2. Regional Wind Speed

Surface wind speed in the dust source regions may also be a potential indicator of surface turbulence that could entrain dust particles into the middle upper troposphere [Chomette *et al.*, 1999]. For instance, Liu *et al.* [2004] found a significant correlation between surface wind speeds and dust outbreaks over the northern China, which means that increases of near-surface wind speeds lead to more dust outbreaks and vice versa. Recent studies indicated that surface wind speed is the most important climatic factor for spring dust storm occurrence over the Tarim Basin [Li *et al.*, 2008]. In this paper, we calculated the correlations between the Miaoergou log-Dust and surface wind speeds recorded by meteorological stations over the



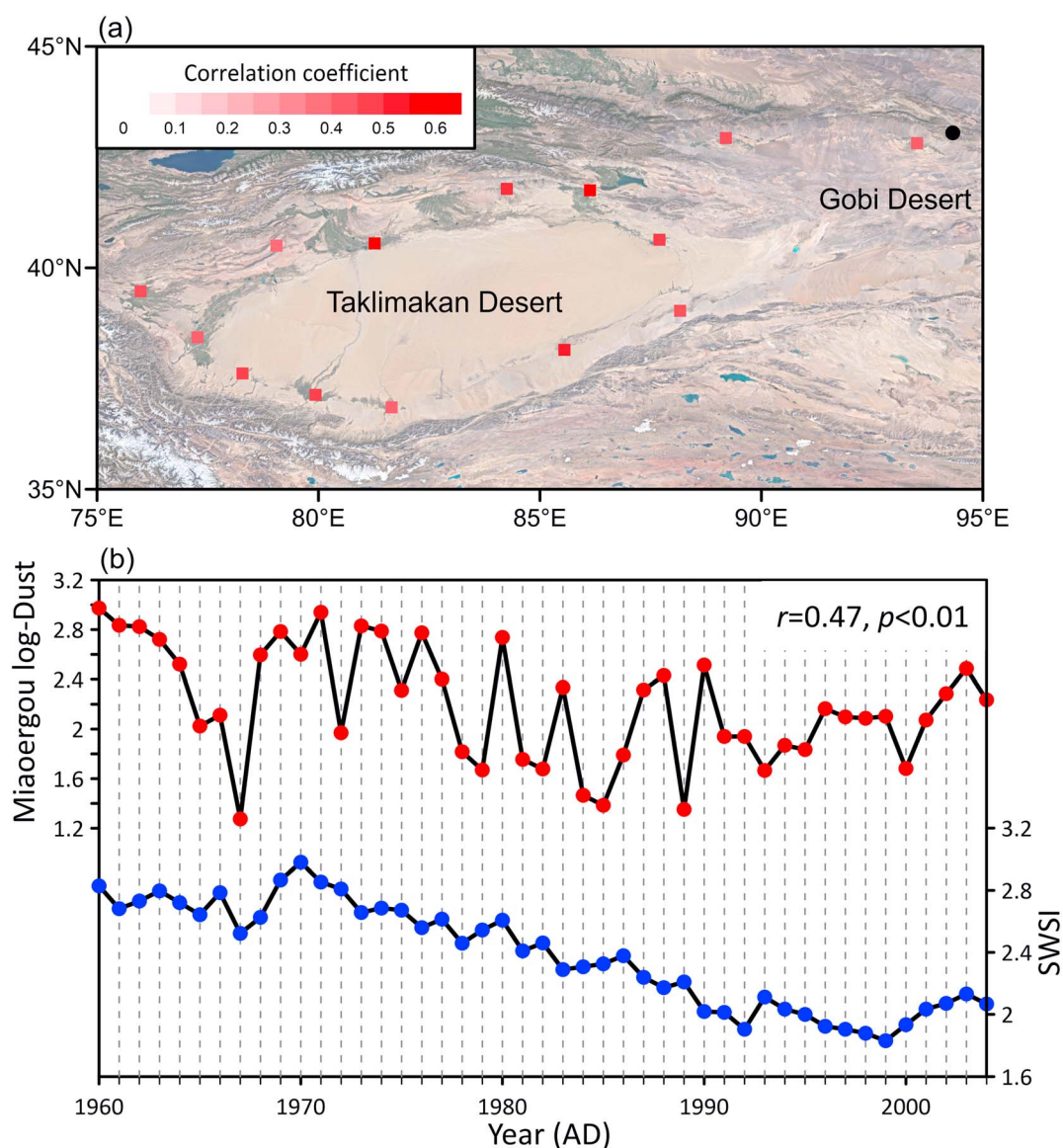


**Figure 6.** (a) Correlations between the Miaoergou log-Dust and the spring surface wind records from the meteorological stations over the Taklimakan desert. The black dot indicates the Miaoergou ice core site. (b) Comparison of the Miaoergou log-Dust with the spring SWSI series.

1960–2004 A.D. We find a significantly positive correlation between the Miaoergou log-Dust and surface wind speeds during the high-frequency dust storm season (March–May) over the Taklimakan desert (Figure 6a). If the averaged near-surface wind speed over the Taklimakan desert is defined as a surface wind speed index (SWSI), there is a strong correlation between variations of the Miaoergou log-Dust and SWSI (Figure 6b). This suggests that surface wind speed is an important factor for controlling dust emission.

#### 4.3.3. Atmospheric Circulation

In addition to the regional and local climate factors mentioned above, large-scale anomalous atmospheric circulations may have an important influence on dust emission through changing the background dynamical conditions [Ding and Li, 2005; Gao and Washington, 2010]. The correlation between the Miaoergou log-Dust and 500 hPa geopotential height in spring over 1948–2004 A.D. shows a significant negative center located in the Mongolia and northwestern China, with a correlation coefficient lower than  $-0.5$  ( $p < 0.01$ ) (Figure 7a). This suggests that the high dust emissions over the northwestern China are closely associated with the negative 500 hPa geopotential height anomalies over this region, and vice versa.

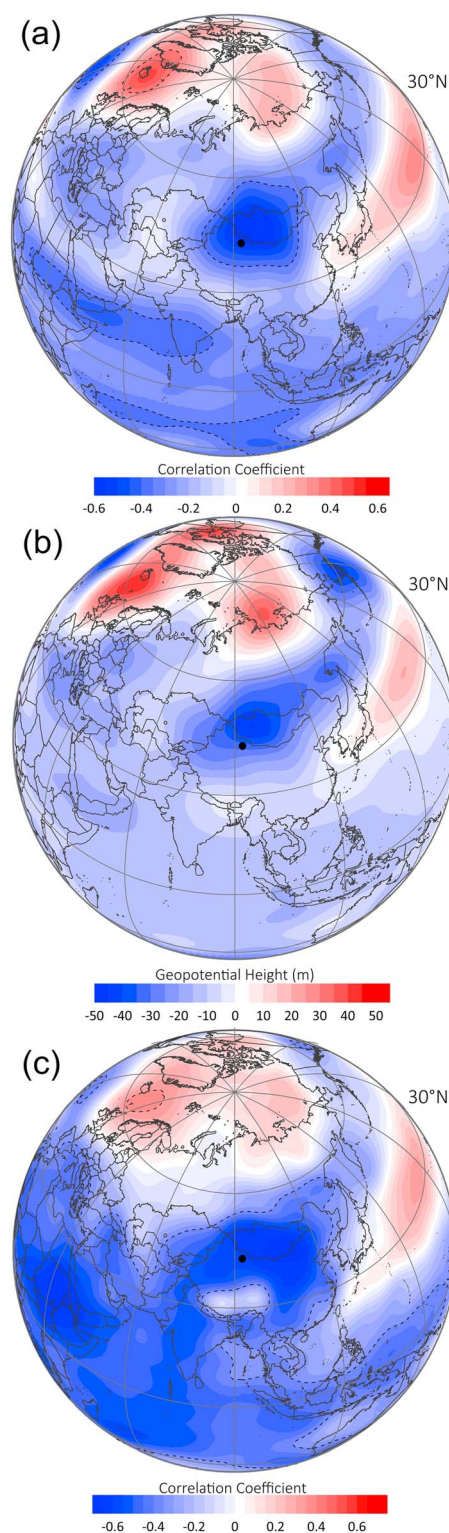


**Figure 7.** (a) Spatial correlations between the Miaoergou log-Dust and spring 500 geopotential height (1948–2004 A.D.) and (c) spring 850 geopotential height (1948–2004 A.D.). (b) Composite difference in the spring 500 hPa geopotential height (m) between years with high and low dust fluxes. The regions circled by black dashed lines in Figures 7a and 7c represent grids with correlations significant at the 99% confidence level. The black dot indicates the Miaoergou ice core site.

We also performed a composite analysis of spring 500 hPa geopotential height. The 10 years with extremely high dust fluxes (1950, 1958, 1959, 1960, 1961, 1962, 1971, 1973, 1974, and 1976) and 10 years with extremely low dust fluxes (1967, 1979, 1982, 1984, 1985, 1986, 1989, 1993, 1995, and 2000) during 1948–2004 A.D. were selected. High dust flux years occurred before the 1980s. Low dust flux years mainly occurred after the 1980s. Results of the composite analysis are presented in Figure 7b, which shows the difference of spring 500 hPa geopotential height between years with higher and lower dust flux. In the years with extremely high (low) dust fluxes, the negative (positive) geopotential height anomaly over the western and central part of Mongolia causes anomalous southerly (northerly) winds over the eastern part of China, and anomalous northerly (southerly) and westerly (westerly) winds over the northwestern China. This pattern tends to enhance (weaken) the intensity of northwest cold air flow from higher latitudes to the northwestern China (Figure S7). Therefore, the changes in the spring 500 hPa geopotential height may provide a large-scale dynamical condition favorable to the low dust emissions over the arid regions over the northwestern China since 1980s.

In addition, we investigated possible link between the Miaoergou log-Dust and 850 hPa geopotential height in spring over 1948–2004 A.D. (Figure 7c). The area with significant correlations coincides with the general position of the Siberian High, which has strong impacts on regional atmospheric circulation patterns [Aizen *et al.*, 1997]. The negative correlations between 850 hPa geopotential height and the Miaoergou log-Dust indicate that as pressure is

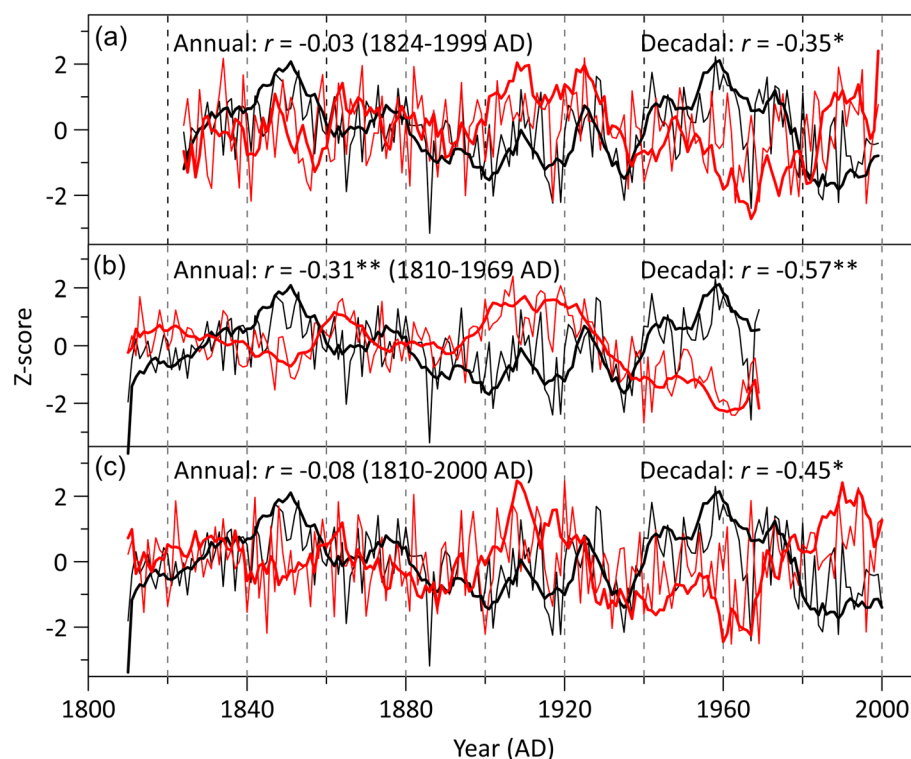


**Figure 8.** (a) Comparison of the Mioergou log-Dust (black lines) with the winter NAO series (red lines) from instrumental measurement in *Vinther et al.* [2003], (b) reconstruction in *Ortega et al.* [2015], and (c) reconstruction in *Luterbacher et al.* [2001]. Thin lines indicate annual series, and thick lines represent running average (11 year running mean for Figures 8a and 8b and 30 year running mean for Figure 8c). The series used for comparison were standardized over their common period of 1824–1999 A.D. (Figure 8a), 1810–1969 A.D. (Figure 8b), and 1810–2000 A.D. (Figure 8c). Correlations between them are shown in each panel. Single (double) asterisk denotes the correlation significant at 95% (99%) confidence level.

reduced, atmospheric dust concentrations increase. Relatively lower pressure may be associated with enhanced regional cyclonic activity and/or a weakening or shift in the strength and position of the SH [Grigholm et al., 2017].

#### 4.3.4. Linkage With the NAO

The NAO is the major large-scale mode of atmospheric variability over the extratropical Atlantic Ocean. It refers to a large-scale seesaw of atmospheric mass between the subtropical high (centered on the Azores) and subpolar low (centered on Iceland) over the Atlantic Ocean [Hurrell et al., 2003]. During the positive phases of NAO, the subtropical Azores high and subpolar Icelandic low are both reinforced, resulting in a stronger north-south pressure gradient. During the negative phases, opposite effects are observed. The NAO is known to profoundly influence the climate variability over the wintertime Northern Hemisphere [Delworth et al., 2016; Luo et al., 2016; Mori et al., 2014] and even the following spring's atmospheric circulations [Li et al., 2016; Zhao et al., 2013]. Previous observational analyses found a negative relationship between the winter NAO and the frequency of spring dust storms in the northwestern China [Fan and Wang, 2004; Zhao et al., 2013]. Zhao et al. [2012] pointed out that the NAO may have an important influence on the Asian climate and the Tibetan glacier records. A recent study indicates that the winter NAO may be connected to atmospheric dust loading over the inner TP [Zhang et al., 2015].

To investigate whether the winter NAOs have influenced the dust emissions over the deserts in the northwestern China (Taklimakan desert) over a longer period, we compared the Mioergou log-Dust with one instrumental and two reconstructed winter NAO series [Luterbacher et al., 2001; Ortega et al., 2015; Vinther et al., 2003].

As shown in Figure 8, there is a significant negative correlation between the Mioergou log-Dust and the instrumental NAO index at multidecadal timescales during 1823–1999 A.D. [Vinther et al., 2003]. The NAO



reconstruction of Luterbacher *et al.* [2001] was developed based on instrumental station pressure, temperature, and precipitation measurements plus documentary proxy data, spanning 1658–2000 A.D., whereas Ortega *et al.* [2015] employed a diverse multiproxy data set comprising ice cores, lake sediment, speleothems, tree rings, and other assorted proxy records over the past 1000 years. The Miaoergou log-Dust showed out-of-phase fluctuations with the two reconstructed NAO series on multidecadal timescales throughout the past two centuries. The correlations between these series and their decadal series are all significant at the 0.05 level, as estimated using Student's *t* tests. A possible physical mechanism for this link lies on how the winter NAO affects local climate factors over the northwestern China. A positive phase of the winter NAO leads to an increase in surface air temperature, soil temperature, and rainfall in most parts of Eurasia in winter [Li *et al.*, 2016]. These changes tend to produce weaker and thinner snow cover in spring compared to the conditions during the negative NAO phase. As a result, the albedo decreases and the surface air temperature increases over Eurasia (centered on the region around the Lake Baikal) [Li *et al.*, 2016; Zhu *et al.*, 2008], which contributes a decreased meridional air temperature gradient, leading to the weakening of the westerly jet stream [Grigholm *et al.*, 2009; Zhu *et al.*, 2008]. These conditions can then contribute to a decrease of dust storms over the northwestern China [Fan and Wang, 2004].

## 5. Conclusions

This study presents a high-resolution atmospheric dust variability record covering the period of 1810–2004 A.D., as reconstructed from an ice core retrieved from the Miaoergou Glacier in eastern Tien Shan. Our results show that the Miaoergou dust flux time series has three periods of relatively low dust flux (i.e., 1810–1829 A.D., 1863–1940 A.D., and 1979–2004 A.D.) and two periods of relatively high dust values (i.e., 1830–1862 A.D. and 1941–1978 A.D.). The result represents large-scale dust emission variations in the deserts between the Tien Shan and Kunlun Mountains. Spatial correlation analyses show that regional factors that contribute to dust emission include annual precipitation, spring soil moisture, and spring surface wind speed. The winter NAO is likely to be an important forcing of dust deposition on the glaciers of eastern Tien Shan over the past two centuries.

## Acknowledgments

This research was supported by the Natural Science Foundation of China (41330526 and 41711530148) and the Chinese Academy of Sciences (XDB03030101-4). The authors gratefully acknowledge the NOAA Air Resource Laboratory (ARL) for the provision of the HYSPLIT transport and dispersion model and/or READY website (<http://www.ready.noaa.gov>) used in this publication. To better facilitate readers to understand the results, the data utilized in this manuscript are presented in Data Set S1.

## References

- Aizen, V. B., E. M. Aizen, J. Dozier, J. M. Melack, D. D. Sexton, and V. N. Nesterov (1997), Glacial regime of the highest Tien Shan Mountain, Pobeda-Khan Tengry massif, *J. Glaciol.*, 43(145), 503–512.
- Aizen, V. B., E. M. Aizen, D. Joswiak, K. Fujita, N. Takeuchi, and S. Nikitin (2006), Climatic and atmospheric circulation pattern variability from ice-core isotope/geochemistry records (Altai, Tien Shan and Tibet), *Ann. Glaciol.*, 43, 49–60, doi:10.3189/172756406781812078.
- Bi, H., J. Ma, W. Zheng, and J. Zeng (2015), Comparison of soil moisture in GLDAS model simulations and in situ observations over the Tibetan Plateau, *J. Geophys. Res. Atmos.*, 121, 2658–2678, doi:10.1002/2015JD024131.
- Chen, J., G. Li, J. Yang, W. Rao, H. Lu, W. Balsam, Y. Sun, and J. Ji (2007), Nd-Sr isotopic characteristics of Chinese deserts: Implications for the provenances of Asian dust, *Geochim. Cosmochim. AC.*, 71, 3904–3914, doi:10.1016/j.gca.2007.04.033.
- Chomette, O., M. Legrand, and B. Marticorena (1999), Determination of the wind speed threshold for the emission of desert dust using satellite remote sensing in the thermal infrared, *J. Geophys. Res.*, 104(D24), 31,207–31,215, doi:10.1029/1999JD900756.
- Claquin, T., M. Schulz, and Y. J. Balkanski (1999), Modeling the mineralogy of atmospheric dust sources, *J. Geophys. Res.*, 104(D18), 22,243–22,256, doi:10.1029/1999JD900416.
- Delworth, T. L., F. Zeng, G. A. Vecchi, X. Yang, L. Zhang, and R. Zhang (2016), The North Atlantic Oscillation as a driver of rapid climate change in the Northern Hemisphere, *Nat. Geosci.*, 9, 509–512, doi:10.1038/NGEO2738.
- Ding, R., and J. Li (2005), Decadal change of the spring dust storm in northwest China and the associated atmospheric circulation, *Geophys. Res. Lett.*, 32, L02808, doi:10.1029/2004GL021561.
- Dong, Z., X. Qin, J. Ren, D. Qin, X. Cui, and J. Chen (2013), A 47-year high resolution chemistry record of atmospheric environment change from the Lanzhou Glacier No. 12, north slope of Qilian Mountains, China, *Quat. Int.*, 313, 137–146, doi:10.1016/j.quaint.2013.09.033.
- Du, Z., C. Xiao, Y. Liu, and G. Wu (2015), Geochemical characteristics of insoluble dust as a tracer in an ice core from Miaoergou Glacier, east Tien Shan, *Global Planet. Change*, 127, 12–21, doi:10.1016/j.gloplacha.2015.01.011.
- Fan, K., and H. J. Wang (2004), Antarctic oscillation and the dust weather frequency in North China, *Geophys. Res. Lett.*, 31, L10201, doi:10.1029/2004GL019465.
- Gao, H., and R. Washington (2010), Arctic oscillation and the interannual variability of dust emissions from the Tarim Basin: A TOMS AI based study, *Clim. Dyn.*, 35, 511–522, doi:10.1007/s00382-009-0687-4.
- Ginoux, P., J. M. Prospero, T. E. Gill, N. C. Hsu, and M. Zhao (2012), Global-scale attribution of anthropogenic and dust sources and their emission rates based on MODIS Deep Blue aerosol products, *Rev. Geophys.*, 50, RG3005, doi:10.1029/2012RG000388.
- Griffin, D. W., C. A. Kellogg, and E. A. Shinn (2001), Dust in the wind: Long range transport of dust in the atmosphere and its implications for global public and ecosystem health, *Global Change Hum. Health*, 2(1), 20–33, doi:10.1023/A:1011910224374.
- Grigholm, B., P. A. Mayewski, S. Kang, Y. Zhang, S. Kaspari, S. B. Sneed, and Q. Zhang (2009), Atmospheric soluble dust records from a Tibetan ice core: Possible climate proxies and teleconnection with the Pacific Decadal Oscillation, *J. Geophys. Res.*, 114, D20118, doi:10.1029/2008JD011242.



- Grigholm, B., et al. (2015), Twentieth century dust lows and the weakening of the westerly winds over the Tibetan Plateau, *Geophys. Res. Lett.*, **42**, 2434–2441, doi:10.1002/2015GL063217.
- Grigholm, B., P. A. Mayewski, V. Aizen, K. Kreutz, C. P. Wake, E. Aizen, S. Kang, K. A. Maasch, M. J. Handley, and S. B. Sneed (2016), Mid-twentieth century increases in anthropogenic Pb, Cd and Cu in central Asia set in hemispheric perspective using Tien Shan ice core, *Atmos. Environ.*, **131**, 17–28, doi:10.1016/j.atmosenv.2016.01.030.
- Grigholm, B., P. A. Mayewski, V. Aizen, K. Kreutz, E. Aizen, S. Kang, K. A. Maasch, and S. B. Sneed (2017), A twentieth century major soluble ion record of dust and anthropogenic pollutants from Inilchek Glacier, Tien Shan, *J. Geophys. Res. Atmos.*, **122**, 1884–1900, doi:10.1002/2016JD025407.
- Harris, I., P. D. Jones, T. J. Osborn, and D. H. Lister (2014), Updated high-resolution grids of monthly climatic observations-the CRU TS3. 10 Dataset, *Int. J. Climatol.*, **34**(3), 623–642, doi:10.1002/joc.3711.
- Hurrell, J. W., Y. Kushnir, G. Ottersen, and M. Visbeck (Eds.) (2003), *The North Atlantic Oscillation: Climatic Significance and Environmental Impact*, vol. 134, 279 pp., AGU, Washington, D. C.
- Intergovernmental Panel on Climate Change (2013), *Climate Change 2013: The Physical Science Basis. Contribution of Working Group I to the Fifth Assessment Report of the Intergovernmental Panel on Climate Change*, edited by T. F. Stocker et al., 595 pp., Cambridge Univ. Press, Cambridge, U. K., and New York, doi:10.1017/CBO9781107415324.
- Ji, Z., S. Kang, Q. Zhang, Z. Cong, P. Chen, and M. Sillanpää (2016), Investigation of mineral aerosols radiative effects over High Mountain Asia in 1990–2009 using a regional climate model, *Atmos. Res.*, **178**–179, 484–496, doi:10.1016/j.atmosres.2016.05.003.225.
- Jickells, T. D., et al. (2005), Global iron connections between desert dust, ocean biogeochemistry, and climate, *Science*, **308**(5718), 67–71, doi:10.1126/science.1105959.
- Kalnay, E., et al. (1996), The NCEP/NCAR 40-year reanalysis project, *Bull. Am. Meteorol. Soc.*, **77**, 437–471.
- Kang, S., P. A. Mayewski, Y. Yan, D. Qin, T. Yao, and J. Ren (2003), Dust records from three ice cores: Relationships to spring atmospheric circulation over the Northern Hemisphere, *Atmos. Environ.*, **37**(34), 4823–4835, doi:10.1016/j.atmosenv.2003.08.010.
- Kang, S., Y. L. Zhang, Y. J. Zhang, B. Grigholm, S. Kaspari, D. Qin, J. Ren, and P. Mayewski (2010), Variability of atmospheric dust loading over the central Tibetan Plateau based on ice core glaciochemistry, *Atmos. Environ.*, **44**(25), 2980–2989, doi:10.1016/j.atmosenv.2010.05.014.
- Kim, H., and M. Choi (2015), Impact of soil moisture on dust outbreaks in East Asia: Using satellite and assimilation data, *Geophys. Res. Lett.*, **42**, 2789–2796, doi:10.1002/2015GL063325.
- Lee, K., S. D. Hur, S. Hou, S. Hong, X. Qin, J. Ren, Y. Liu, K. J. R. Rosman, C. Barbante, and C. F. Boutron (2008), Atmospheric pollution for trace elements in the remote high-altitude atmosphere in central Asia as recorded in snow from Mt. Qomolangma (Everest) of the Himalayas, *Sci. Total Environ.*, **404**, 171–181, doi:10.1016/j.scitotenv.2008.06.022.
- Li, H., J. Li, and Q. He (2008), Study on sandstorm trend and abrupt change in Xinjiang [in Chinese with English abstract], *J. Desert Res.*, **25**, 915–919.
- Li, J., K. Fan, and Z. Xu (2016), Links between the late wintertime North Atlantic Oscillation and springtime vegetation growth over Eurasia, *Clim. Dyn.*, **46**, 987–1000, doi:10.1007/s00382-015-2627-9.
- Liu, X., Z. Yin, X. Zhang, and X. Yang (2004), Analyses of the spring dust storm frequency of northern China in relation to antecedent and concurrent wind, precipitation, vegetation, and soil moisture conditions, *J. Geophys. Res.*, **109**, D16210, doi:10.1029/2004JD004615.
- Liu, Y., S. Hou, Y. Wang, and L. Song (2009), Distribution of borehole temperature at four high-altitude alpine glaciers in central Asia, *J. Mt. Sci.*, **6**(3), 221–227, doi:10.1007/s11629-009-0254-9.
- Liu, Y., S. Hou, S. Hong, S. D. Hur, K. Lee, and Y. Wang (2011), High-resolution trace element records of an ice core from the eastern Tien Shan, central Asia, since 1953 A.D., *J. Geophys. Res.*, **116**, D12307, doi:10.1029/2010JD015191.
- Luo, D., Y. Xiao, Y. Diao, A. Dai, C. L. E. Franzke, and I. Simmonds (2016), Impact of Ural blocking on winter warm Arctic-cold Eurasian anomalies. Part II: The link to the North Atlantic Oscillation, *J. Clim.*, **29**, 3949–3971, doi:10.1175/JCLI-D-15-0612.1.
- Luterbacher, J., et al. (2001), Extending North Atlantic Oscillation reconstructions back to 1500, *Atmos. Sci. Lett.*, **2**, 114–124, doi:10.1006/asle.2001.0044.
- McTainsh, G. H. A., W. Lynch, and E. K. Tew (1998), Climatic controls upon dust storm occurrence in eastern Australia, *J. Arid Environ.*, **39**(3), 457–466, doi:10.1006/jare.1997.0373.
- Meji, R. (1994), Trace element behavior in coal-fired power plant, *Fuel Process. Technol.*, **39**, 199–217.
- Mori, M., M. Wasahiro, H. Shiogama, J. Inoue, and M. Kimoto (2014), Robust Arctic sea-ice influence on the frequent Eurasian cold winters in past decades, *Nat. Geosci.*, **7**, 869–873, doi:10.1038/ngeo2277.
- Ortega, P., F. Lehner, D. Swingedouw, V. Mass-Delmotte, C. C. Raible, M. Casado, and P. Yiou (2015), A model-tested North Atlantic Oscillation reconstruction for the past millennium, *Nature*, **523**, 71–74, doi:10.1038/nature14518.
- Osborn, T. J., J. Barichivich, I. Harris, G. Schrier, and P. D. Jones (2016), Monitoring global drought using the self-calibrating Palmer Drought Severity Index [in “State of the Climate in 2015”], *Bull. Am. Meteorol. Soc.*, **96**(7), S30–S31.
- Parungo, F., Z. Li, X. Li, D. Yang, and J. Harris (1994), Gobi dust storms and the Great Green Wall, *Geophys. Res. Lett.*, **21**(11), 999–1002, doi:10.1029/94GL00879.
- Prospero, J. M., P. Ginoux, O. Torres, S. E. Nicholson, and T. E. Gill (2002), Environmental characterization of global sources of atmospheric soil dust identified with the Nimbus 7 Total Ozone Mapping Spectrometer (TOMS) absorbing aerosol product, *Rev. Geophys.*, **40**(1), 1002, doi:10.1029/2000RG000095.
- Rao, W., H. Tan, J. Chen, J. Ji, Y. Chen, Y. Pan, and W. Zhang (2015), Nd–Sr isotope geochemistry of fine-grained sands in the basin-type deserts, West China: Implications for the source mechanism and atmospheric transport, *Geomorphology*, **246**, 458–471, doi:10.1016/j.geomorph.2015.06.043.
- Rodell, M., et al. (2004), The global land data assimilation system, *Bull. Am. Meteorol. Soc.*, **85**(3), 381–394, doi:10.1175/BAMS-85-3-381.
- Rosenfeld, D., Y. Rudich, and R. Lahav (2001), Desert dust suppressing precipitation: A possible desertification feedback loop, *Proc. Natl. Acad. Sci. U.S.A.*, **98**(11), 5975–5980, doi:10.1073/pnas.101122798.
- Schrier, G., J. Barichivich, K. R. Briffa, and P. D. Jones (2013), A scPDSI-based global data set of dry and wet spells for 1901–2009, *J. Geophys. Res. Atmos.*, **118**, 4025–4048, doi:10.1002/jgrd.50355.
- Shi, Y., S. Liu, B. Ye, C. Liu, and Z. Wang (2008), *Concise Glacier Inventory of China*, pp. 116–135, Shanghai Pop. Sci. Press, Shanghai, China.
- Sun, J., M. Zhang, and T. Liu (2001), Spatial and temporal characteristics of dust storms in China and its surrounding regions, 1960–1999: Relations to source area and climate, *J. Geophys. Res.*, **106**(D10), 10,325–10,333, doi:10.1029/2000JD900665.
- Tenzin, D., T. Yao, P. Yao, U. Deji, B. Xu, H. Zhao, and M. Zhu (2016), Variation of atmospheric dust over the past 100 years recorded by visible dusty layers of the Kuokuosele ice core, western Tibetan Plateau, *Chin. Sci. Bull.*, **61**(15), 1695–1705, doi:10.1360/N972015-01309.

- Thompson, L. G., T. Yao, E. Mosley-Thompson, M. E. Davis, K. A. Henderson, and P. N. Lin (2000), A high-resolution millennial record of the South Asian monsoon from Himalayan ice cores, *Science*, 289, 1916–1919, doi:10.1126/science.289.5486.1916.
- Thompson, L. G., E. Mosley-Thompson, H. Brecher, M. Davis, B. Leon, D. Les, P.-N. Lin, T. Mashiotta, and K. Mountain (2006), Abrupt tropical climate change: Past and present, *Proc. Natl. Acad. Sci. U.S.A.*, 103(28), 10,536–10,543, doi:10.1073/pnas.0603900103.
- Uno, I., K. Eguchi, K. Yumimoto, T. Takemura, A. Shimizu, M. Uematsu, Z. Liu, Z. Wang, Y. Hara, and N. Sugimoto (2009), Asian dust transported one full circuit around the globe, *Nat. Geosci.*, 2(8), 557–560, doi:10.1038/NGEO583.
- Vinther, B. M., K. K. Andersen, A. W. Hansen, T. Schmidth, and P. D. Jones (2003), Improving the Gibraltar/Reykjavik NAO index, *Geophys. Res. Lett.*, 30(23), 2222, doi:10.1029/2003GL018220.
- Wake, C. P., and P. A. Mayewski (1994), Modern eolian dust deposition in central Asia, *Tellus B*, 46, 220–233, doi:10.1034/j.1600-0889.1994.t012-2-00005.x.
- Wang, C., S. Hou, H. Pang, Y. Liu, H. W. Gäggeler, L. Tobler, S. Szidat, and E. Vogel (2014),  $^{210}\text{Pb}$  dating of the Miaoergou ice core from the eastern Tien Shan, China, *Ann. Glaciol.*, 55(66), 105–110, doi:10.3189/2014AoG66A151.
- Wang, C., Y. Liu, W. Zhang, S. Hong, S. D. Hur, K. Lee, H. Pang, and S. Hou (2016), High-resolution atmospheric cadmium record for A.D. 1776–2004 in a high-altitude ice core from the eastern Tien Shan, central Asia, *Ann. Glaciol.*, 57(71), 265–272, doi:10.3189/2016AoG71A501.
- Wang, N. (2005), Decrease trend of dust event frequency over the past 200 years recorded in the Malan ice core from the northern Tibetan Plateau, *Chin. Sci. Bull.*, 50(24), 2866–2871, doi:10.1360/982005-237.
- Wu, G., C. Zhang, X. Zhang, L. Tian, and T. Yao (2010a), Sr and Nd isotopic composition of dust in Dunde ice core, Northern China: Implications for source tracing and use as an analogue of long-range transported Asian dust, *Earth Planet. Sci. Lett.*, 299(3), 409–416, doi:10.1016/j.epsl.2010.09.021.
- Wu, G., T. Yao, B. Xu, L. Tian, C. Zhang, and X. Zhang (2010b), Dust concentration and flux in ice cores from the Tibetan Plateau over the past few decades, *Tellus B*, 62(3), 197–206, doi:10.1111/j.1600-0889.2010.00457.x.
- Wu, G., C. Zhang, B. Xu, R. Mao, D. Joswiak, N. Wang, and T. Yao (2013), Atmospheric dust from a shallow ice core from Tanggula: Implications for drought in the central Tibetan Plateau over the past 155 years, *Quat. Sci. Rev.*, 59, 57–66, doi:10.1016/j.quascirev.2012.10.003.
- Xu, J., S. Hou, D. Qin, S. Kang, J. Ren, and J. Ming (2007), Dust storm activity over the Tibetan Plateau recorded by a shallow ice core from the north slope of Mt. Qomolangma (Everest), Tibet-Himal region, *Geophys. Res. Lett.*, 34, L17504, doi:10.1029/2007GL030853.
- Xu, J., S. Hou, F. Chen, J. Ren, and D. Qin (2009), Tracing the sources of particles in the Earth Rongbuk ice core from Mt. Qomolangma, *Chin. Sci. Bull.*, 54(10), 1781–1785, doi:10.1007/s11434-009-0050-5.
- Xu, J., et al. (2010), A 108.83-m ice-core record of atmospheric dust deposition at Mt. Qomolangma (Everest), central Himalaya, *Quat. Res.*, 73, 33–38, doi:10.1016/j.yqres.2009.09.005.
- Xu, J., G. Yu, S. Kang, S. Hou, Q. Zhang, J. Ren, and D. Qin (2012), Sr-Nd isotope evidence for modern aeolian dust sources in mountain glaciers of western China, *J. Glaciol.*, 58(211), 859–865, doi:10.3189/2012JoG12J006.
- Xu, J., S. Kang, S. Hou, Q. Zhang, J. Huang, C. Xiao, J. Ren, and D. Qin (2016), Characterization of contemporary aeolian dust deposition on mountain glaciers of western China, *Sci. Cold Arid Reg.*, 8(1), 9–21, doi:10.3724/SP.J.1226.2016.00009.
- Zhang, W., S. Hou, W. An, L. Zhou, and H. Pang (2016), Variations in atmospheric dust loading since A.D. 1951 recorded in an ice core from the northern Tibetan Plateau, *Ann. Glaciol.*, 57(71), 258–264, doi:10.3189/2016AoG71A559.
- Zhang, Y., et al. (2015), A 500 year atmospheric dust deposition retrieved from a Mt. Geladaindong ice core in the central Tibetan Plateau, *Atmos. Res.*, 166, 1–9, doi:10.1016/j.atmosres.2015.06.007.
- Zhao, H., B. Xu, T. Yao, G. Wu, S. Liu, J. Gao, and M. Wang (2012), Deuterium excess record in a southern Tibetan ice core and its potential climatic implications, *Clim. Dyn.*, 38, 1791–1803, doi:10.1007/s00382-011-1161-7.
- Zhao, W., Y. Sun, W. Balsam, L. Zeng, H. Lu, K. Otgonbayar, and J. Ji (2015), Clay-sized Hf-Nd-Sr isotopic composition of Mongolian dust as a fingerprint for regional to hemispherical transport, *Geophys. Res. Lett.*, 42, 5661–5669, doi:10.1002/2015GL064357.
- Zhao, Y., A. Huang, X. Zhu, Y. Zhou, and Y. Huang (2013), The impact of the winter North Atlantic Oscillation on the frequency of spring dust storms over Tarim Basin in northwest China in the past half-century, *Environ. Res. Lett.*, 8(2), 024026, doi:10.1088/1748-9326/8/2/024026.
- Zhu, C., B. Wang, and W. Qian (2008), Why do dust storms decrease in northern China concurrently with the recent global warming?, *Geophys. Res. Lett.*, 35, L18702, doi:10.1029/2008GL034886.